Nanoscale Research Letters

NANO EXPRESS Open Access

UV-Visible Photodetector Based on I-type Heterostructure of ZnO-QDs/Monolayer MoS_2

Yong Heng Zhou, Zhi Bin Zhang, Ping Xu, Han Zhang and Bing Wang*

Abstract

Monolayer MoS_2 has shown excellent photoresponse properties, but its promising applications in high-sensitivity photodetection suffer from the atomic-thickness-limited adsorption and band gap-limited spectral selectivity. Here we have carried out investigations on MoS_2 monolayer-based photodetectors with and without decoration of ZnO quantum dots (ZnO-QDs) for comparison. Compared with monolayer MoS_2 photodetectors, the monolayer ZnO-QDs/MoS_2 hybrid device exhibits faster response speed (1.5 s and 1.1 s, respectively), extended broadband photoresponse range (deep UV-visible), and enhanced photoresponse in visible spectrum, such as higher responsivity over 0.084 A/W and larger detectivity of 1.05×10^{11} Jones, which results from considerable injection of carries from ZnO-QDs to MoS_2 due to the formation of I-type heterostructure existing in the contact interface of them.

Keywords: Photodetector, 2D materials, I-type heterostructure

Highlights

1. Monolayer MoS_2 has shown excellent photoresponse properties.
2. ZnO-QDs/MoS_2 hybrid device exhibits faster response speed, extended broadband photoresponse range and enhanced photoresponse in visible spectrum.
3. I-type heterostructure existing in the contact interface of ZnO-QDs/MoS_2.

Introduction

Broadband photodetectors are important components of optoelectronic systems, optical communication, environmental monitoring, and so on [1–5]. Especially, UV-visible photodetectors, one of the important broadband photodetectors, have been used in biomedical imaging systems, ultraviolet astronomy, wide spectral switches, memory storage, etc. [6–8]. Therefore, it is very necessary to fabricate various materials with highly effective photoresponse in this broadband region [9, 10]. As one of the most studied transition metal dichalcogenide (TMD), 2D molybdenum disulfide (MoS_2) has presented outstanding potential for constructing various of electronic and optoelectronic devices due to reduced dimensionality [11–13], high carrier mobility, strong electron-hole confinement, and high-light sensitivity [14–16]. However, owing to narrower band gap of 1.8 eV for the monolayer, MoS_2 usually exhibits excellent light absorption to green light region rather than UV-visible range. In order to achieve this broadband photoresponse range, one of the most effective solutions is the construction of heterojunction with other semiconductors owning larger band gap, which can not only extend the response range to UV region from visible range but also inject photoexcited carriers so as to greatly improve the photo gain.

Type II heterojunction is the most widely studied type of two-dimensional material-based photodetectors, in which built-in electric fields can separate carriers efficiently and thus enhance photocurrent, but the recombination time of carriers is also prolonged, leading to slow response time. By comparison, the energy band structure

* Correspondence: wangbing@szu.edu.cn
College of Physical and Optoelectronic Engineering; College of Electronics and Information Engineering; Institute of Micro-nano Optoelectronic Technology; SZU-NUS Collaborative Innovation Centre for Optoelectronic Science & Technology; Key Laboratory of Optoelectronic Devices and Systems of Ministry of Education and Guangdong Province, Shenzhen University, Shenzhen 518060, Guangdong, People's Republic of China

of type I heterojunction allows charges inject from one larger band gap material to another narrower band gap material which leads to the accumulation of charges in the narrower band gap material. Moreover, charges confined inside the material can increase the carrier recombination efficiency so that devices based on it will have a faster response time. Due to the above merits, considerable attention has been paid to type I heterojunction, especially heterojunction formed between the QDs and the layered materials. These 2D-0D hybrid architectures have recently been brought into focus for their high performance as photodetectors because of this structure boosting enhancement of light absorption, facilitating band gap tunability, decreasing the response and decay time, and promoting the concentration of photoexcited charges induced by I-type heterojunction formed between the QDs and the layered materials [17–19].

Among several wide band gap semiconductors, zinc oxide (ZnO) has been a well-established material for UV photodetection due to its wide band gap (3.37 eV), high exciton binding energy (60 meV), and fast switching time on illumination with UV light [1, 20]. Recently, ZnO-QDs have widely applied in optoelectronics owing to unique optical properties, large surface-to-volume ratio, and tunable optical band gap [21, 22]. Furthermore, quantum tunneling combining with charge trapping states occurs on the surface of the ZnO-QDs in virtue of the charge carriers being confined in all the three directions. Hence, it is very crucial to present I-type hybrid heterostructure based on 2D MoS_2 and ZnO-QDs so as to realize the excellent UV-visible broadband photoresponse with high photo absorbance, responsivity, detectivity, EQE, current on/off ratio, and so on.

Herein, we report a photodetector based on monolayer ZnO-QDs/MoS_2 hybrid structure fabricated in a simple process. Due to the I-type heterojunction formed between monolayer MoS_2 and ZnO-QDs, the device exhibits fast response speed, extended broadband photoresponse range (deep UV-visible), enhanced photo absorbance, photoresponse, and detectivity. It is also notable that the responsivity reaches as high as 0.084 A/W under 405-nm light at power density (PD) of 0.073 mW/cm^2, which is comparable with that of hybrid photodetection at the same wavelength [23, 24]. Thus, our study may provide a method to improve the performance of photodetectors and expand the building blocks for high-performance optoelectronic devices.

Method Section

Growth of Triangular Monolayer MoS_2

Molybdenum trioxide (MoO_3, 99.99%) and sulfur (S, 99.5%) were used to synthesize high crystalline triangular MoS_2 flakes on sapphires through chemical vapor deposition (CVD) procedure [7]. As substrates, sapphires were well cleaned in acetone, alcohol, and deionized water with sonication for 10 min, respectively. And then, they were tightly aligned and placed above an alumina boat which contained 3 mg MoO_3 powders, and the boat was placed into the quartz tube and located in the high-temperature region of the furnace. Subsequently, another boat containing 120 mg sulfur (S) powders was placed into the quartz tube too and located in the lower temperature region of the furnace. Before growth, the tube was evacuated by vacuum bump and purged with pure argon (Ar) gas (99.999%) for several times in order to remove oxygen and water in the tube. Next, the temperature of the MoO_3 powder rose to 400 °C and kept this temperature for 10 min, and then, rising to 780 °C. When it reached 650 °C, the temperature of the S powders rose to 150 °C within 5 min. Then, high- and low-temperature region remained ultimate temperatures for 5 and 15 min, respectively, and the tube was flushed with argon gas with a flow rate of 10 sccm. After the furnace was cooled down to room temperature, we got the samples grown on the substrates.

Synthesis of ZnO Quantum Dots

ZnO quantum dots were synthesized by the sol-gel method under room temperature. A total of 0.878 g of Zinc acetate dihydrate ($Zn(Ac)_2{\cdot}2H_2O$) was added in 80 ml triethylene glycol (TEG) in a conical bottle and stirred vigorously; 0.252 g of lithium hydroxide monohydrate ($LiOH{\cdot}H_2O$) was then gradually added into solution. After being stirred for more than 5 h, the solution became clear and green fluorescence could be observed under illumination of UV excitation. If the solution was stirred for 24 h, it exhibited much stronger fluorescence. Next, the bottle was sealed and sonicated in ice water for 30 min. And then, ethyl acetate was added into bottle until precipitates appeared. Ultimately, ZnO quantum dots powdered samples were collected by centrifugation of precipitates, washed by acetone for three times to remove unreacted precursors, heated at 70 °C for 6 h, and dispersed in ethanol for 1 h.

ZnO-QDs/Monolayer MoS_2 Device Fabrication

Conventional photolithography was used to directly fabricate Au/Ti electrodes on the monolayer MoS_2 grown on the sapphire substrates to construct the devices. Positive photoresist was spin coated on sapphire at 4000 rpm for 1 min and baked at 90 °C for 1 min. And then, electrode patterns were made on monolayer MoS_2 by photolithography system. Next, Ti film (5 nm) and Au film (50 nm) were deposited on the substrate one after another by thermal evaporation and followed by lifting off in acetone to remove Ti and Au film which adhered to photoresist so that electrodes formed. After that, devices were annealed at 200 °C for 2 h with a flow

of Ar (100 sccm) to remove residues so as to form better contact between MoS_2 and electrodes. Ultimately, the ZnO-QDs were dispersed in ethanol solution (2 mg/ml) and single droplet was dropped and spin coated over the MoS_2 device at 1000 rpm for 60 s before baked at 70 °C for 10 min; this process being repeated 3 times to ensure that MoS_2 surface was covered by enough ZnO-QDs.

Characterization

Optical images were taken by Motic BA310Met to verify morphology of the as-grown MoS_2. Atomic force microscope (AFM) height data was recorded by Bruker Dimension FastScan. Raman mapping, spectra of Raman, and photoluminescence (PL) were recorded on a Raman system (InVia-Reflex) with a 532-nm excitation laser under ambient conditions. X-ray diffraction (XRD) for crystal structure of ZnO powder samples was measured at speed of 8° min^{-1} by using D8 Advance in situ X-ray powder diffractometer. Transmission electron microscope (TEM) and high-resolution transmission electron microscopy (HRTEM) were examined by FEI Tecnai G2 F30 instrument (200 kV). The sample solutions (2 mg/ml) were dropped on carbon-coated copper grids and put into a vacuum drying oven to dry at 70 °C overnight. UV-Vis diffuse reflectance and absorption spectra were obtained by spectrophotometer (Lambda950, PerkinElmer).

Photoelectric Performance Characterization

Our device was tested in a sealed box to prevent electromagnetic disturbance. DUV to visible lights were generated by lasers (VIASHO). Light spot with diameter of 0.7 cm was perpendicularly irradiated on device to ensure device was fully irradiated. Light power intensity was measured by a power energy meter (Thorlabs PM100D) with a silicon power head (Thorlabs S120VC). All photoelectric measurements were carried out by a source meter (Keithley 2636B).

Results and Discussion

Morphology and Structure of the ZnO-QDs/Monolayer MoS_2 Photodetector

Spin coating of ZnO-QDs solution was adopted to fabricate ZnO-QDs/MoS_2 device, as shown in Fig. 1a. Figure 1b shows the optical image of monolayer MoS_2 flakes with average side length of 25 μm. AFM image in Fig. 1c shows the thickness of MoS_2 flakes is ~ 0.8 nm, indicating these triangle shape MoS_2 flakes are monolayer [25]. Additionally, two Raman active modes located at 384.24 cm^{-1} and 403.18 cm^{-1} shown in Raman spectra in Fig. 1d correspond to in-plane E^1_{2g} and out-of-plane A_{1g}, respectively. The difference of two peaks is 18.94 cm^{-1} next, in PL spectrum shown in Fig. 1e, there is a peak located at 1.84 eV. Both results are distinguishing features of monolayer MoS_2 [26]. Corresponding Raman mapping shown in Fig. 1f indicating that the MoS_2 flake has uniform thickness.

ZnO-QDs can emit light due to spontaneous emission effect, which was observed in our experiment, as shown in Fig. 2b. Figure 2b demonstrates the XRD patterns of powdered ZnO-QDs that in accordance with JCPDS card no. 36-1451 and no other peaks are observed, which not only verifies the existence of ZnO but also means precursors, have been completely removed by acetone. XRD patterns of QDs materials tend to have wider full width at half maximum (FWHM) compared with bulk or powder materials [27], which is also observed in our as-fabricated ZnO powders. In order to ensure the average size and distribution of ZnO-QDs dispersed in ethanol, TEM and HRTEM are used; corresponding images of ZnO-QDs are shown in Fig. 2c and d. The average size of ZnO-QDs is 4.3 ± 1.87 nm; this result is obtained by statistical TEM analysis of over 100 ZnO-QDs. From HRTEM image in Fig. 2d, we find that ZnO-QDs have highly crystal quality with a lattice spacing of 0.28 nm, which corresponds to (100) plane of crystalline ZnO.

Optoelectronic Performance of the ZnO-QDs/Monolayer MoS_2 Photodetectors

Current vs bias voltage (I–V) characteristics of ZnO-QDs/MoS_2 devices in dark and under light illumination (532 nm) are shown in Fig. 3a, and the inset is higher magnification I–V characteristics located at negative voltage. The highest on/off ratio was measured to be about 100 at voltage of 0.5 V. The effective area of the device is 185.71 μm^2 and the laser PD varies from 1.97 to 24.08 mW/cm^2. Due to Schottky contacts between the monolayer MoS_2 and electrodes, the I–V curves is asymmetrical. The advantages of Schottky barrier located at the contact areas are that the Schottky barrier can not only separate photogenerated electron-hole pairs in a shorter time but also reduce the electron-hole recombination rate so as to be beneficial to achieving high photocurrent and fast response speed [28–30]. As PD increased, photocurrent increased significantly when the device was applied with positive voltage, thus all further measurements were performed at V_{ds} = 1 V.

Responsivity is one of the crucial parameters of photodetectors, which is defined by $R_\lambda = I_{ph}/PS$, where P is the light PD, and S is the effective area of the photosensitive. We present a 3D responsivity map of ZnO-QDs/MoS_2 device in Fig. 3b, which reflects the impact of different V_{ds} and PD on responsivity. To find out the performance differences between pristine device and ZnO-QDs decorated device, we measured and compared photocurrent ($I_{ph} = I_{light} - I_{dark}$) plotted by red points and responsivity (R_λ) plotted by green points, under illumination of 405-nm laser with V_{ds} = 1 V, as shown in Fig. 3c. The photocurrent is fitted by $I_{ph} \sim P^\alpha$, where P is

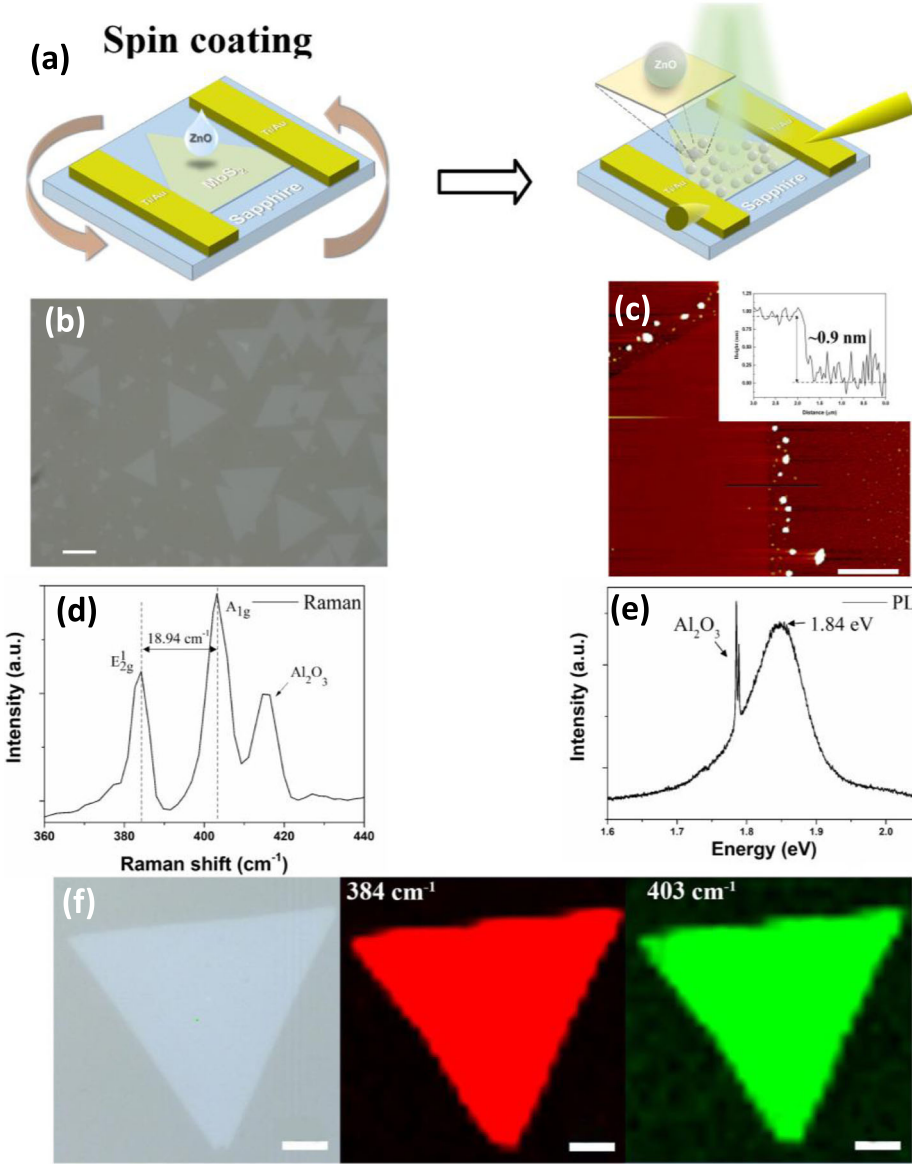

Fig. 1 **a** Schematic diagram of pristine device and ZnO-QDs/MoS_2 device. **b** Optical images of MoS_2 flakes, scale bar, 10 μm. **c** AFM image, the inset shows the thickness of MoS_2, scale bar, 2 μm. **d** Raman spectrum and **e** PL spectrum of the MoS_2 flake. **f** Raman mapping of the MoS_2 flake, scale bar, 5 μm

the light PD and α represents the index of the power law. Fitting the measured photocurrents, the value of α = 0.8 for the pristine MoS_2 and α = 0.84 for ZnO-QDs/MoS_2 are achieved. Here, the calculated α close to 1 implies there are less photoexcited carrier lost due to recombination [31]. The pristine device has maximum photocurrent of 0.168 nA under laser PD of 24.08 mW/cm^2 and exhibits responsivity of 0.028 A/W under lower laser PD of 0.073 mW/cm^2. With the same PD, ZnO-QDs/MoS_2 device shows a higher photocurrent of 0.667 nA and a responsivity of 0.084 A/W. This result reveals photocurrent of monolayer MoS_2 devices can be significantly improved by decoration of ZnO-QDs. Besides, two important parameters in photodetection, external quantum efficiency (EQE) and detectivity (D*), were also calculated for further comparison. EQE is ratio of photogenerated electrons which are collected outside of the device to the number of incident photons, expressed as EQE = $hcR_\lambda/\lambda e$, where h is Planck's constant, c is the speed of light, λ is the wavelength of excitation light, and e is the elementary electronic charge. As for D*, it can quantify the sensitivity of the photodetector and is

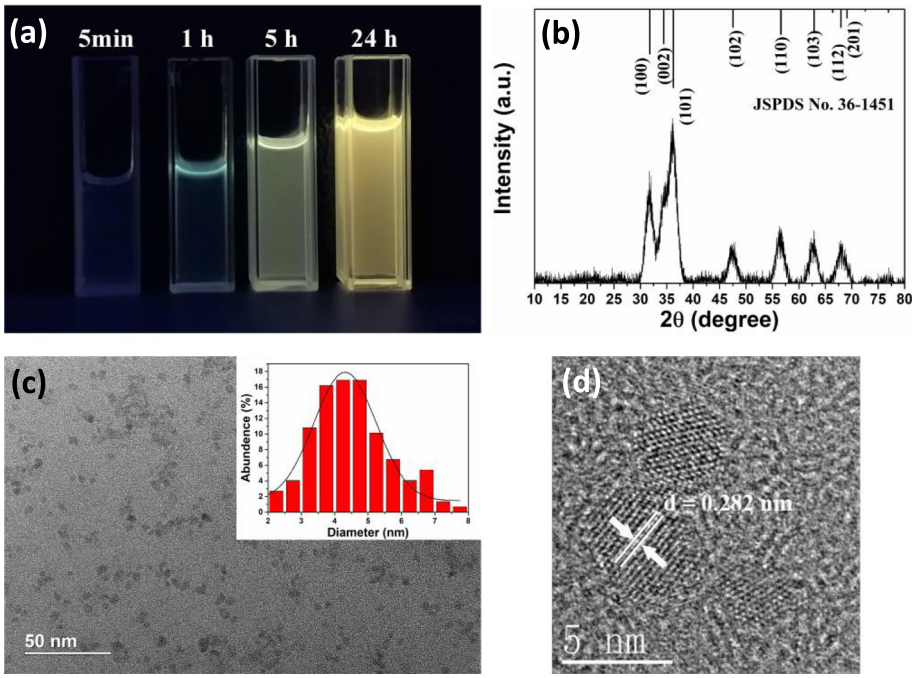

Fig. 2 **a** ZnO-QDs with different synthesis time emitted light under illumination of UV light. **b** XRD diffraction patterns of powdered ZnO-QDs. **c**, **d** TEM and HRTEM images of ZnO-QDs. Inset shows size distribution of ZnO-QDs

defined as $D^* = R_\lambda S^{1/2} / (2eI_{dark})^{1/2}$ if we assume the I_{dark} contributes to major noise. As shown in Fig. 3d, pristine device exhibits a maximum EQE (red) and D* (green), corresponding to 8.5% and 3.84 × 10^{10} Jones, respectively, under laser PD of 0.075 mW/cm^2. Meanwhile, with the same PD, maximum EQE and D*, corresponding to 25.7% and 1.05 × 10^{11} Jones, respectively, both of them being about 3 times higher than those of the pristine one are obtained by ZnO-QDs/MoS_2 device. The D* achieved by our hybrid device is competitive with that of many other reported photodetectors based on layered materials, such as graphene quantum dot/WSe_2/Si heterojunction (4.51 × 10^9 Jones) and graphene/graphene QDs/graphene structure (~ 10^{11} Jones) [32, 33]. This is because I_{dark} obtained in device is reduced to extremely small value below 0.1 nA at 1 V bias; it is comparable with I_{dark} of graphene-silicon heterojunction photodetector (0.1 nA at zero bias) [34].

Photocurrent of pristine device and ZnO-QDs decorated device under exposure of laser with different wavelength are given in Fig. 4a. There exists clear enhancement of photocurrent whatever in 405 nm, 532 nm, or 635 nm, which implies ZnO quantum dots with a wide band gap are able to improve the performance of visible light detection. We further investigated the broadband spectral response of the hybrid device, 254-nm light with PD of 0.26 mW/cm^2 and 375-nm light with PD of 0.51 mW/cm^2 were applied to illuminate hybrid device and excellent photoresponse properties were observed as shown in Fig. 4b. Besides, the hybrid device shows no response when it was illuminated by the light with wavelength over 800 nm. Although the power of UV light illumination is low, the photocurrent is still much higher or at least comparable with those obtained under visible light illumination with much higher PD. We believe it is the wide band gap of ZnO-QDs that allows hybrid device to absorb more photons when UV light falls on it; thus, lots of carries are generated and transferred to MoS_2 so as to greatly enlarge photocurrent. Moreover, after switching on/off status for 6 times over 250 s, photocurrent and dark current still stayed on their level, which demonstrated excellent photo stability of this hybrid device.

A photodetector with fast response speed is suitable of some areas, such as optical communication and video imaging. As another important parameter of photodetectors, response time was also investigated under incident 635-nm light with PD of 35 mW/cm^2. In this work, we defined the rise time and the decay time of the photodetector as the time taken for the device to reach 90% of the equilibrium value from the initial current, and vice versa, respectively. For the pristine device, rise time was 9.5 s and decay time was 17.4 s, such slow response speed mainly due to trap states located in band gap which was introduced by defects in the materials [35]. After MoS_2 photodetector was decorated with ZnO-QDs, as shown in Fig. 4c and d, the rise and decay time reduced to 1.5 s and 1.1 s, the response time was reduced by 84.2% and 93.7%, respectively. This result demonstrates that ZnO-QDs can greatly shorten response time

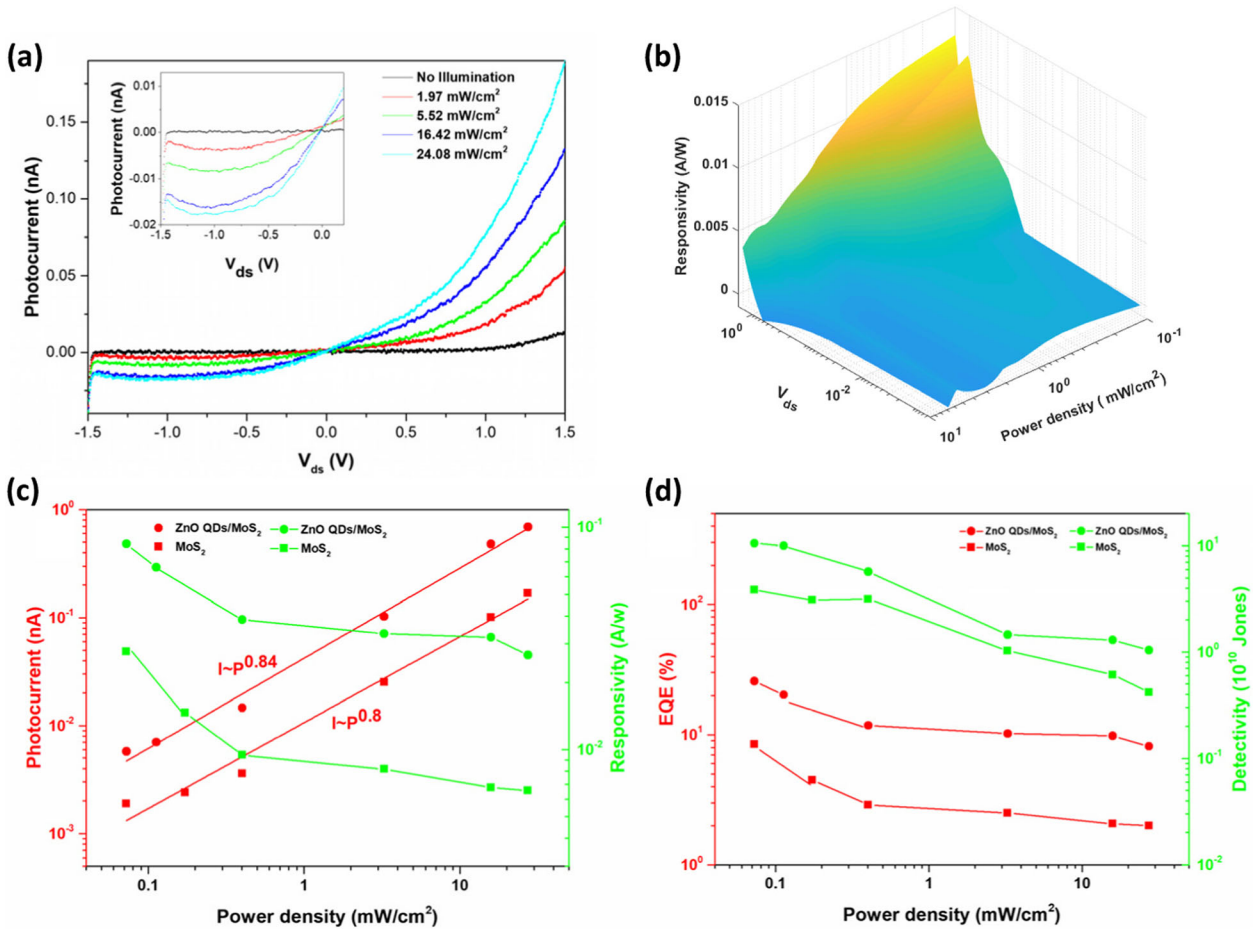

Fig. 3 **a** I–V characteristics of the ZnO-QDs/MoS_2 photodetector under different illumination power densities. Inset is the higher magnification I–V characteristics (negative voltage) under dark and different illumination power densities. **b** 3D responsivity map of the ZnO-QDs/MoS_2 photodetector. **c** Power intensity-dependent photocurrent (red) and responsivity (R, green) under an excitation wavelength of 532 nm at V_{ds} = 1 V. **d** Power intensity-dependent external quantum efficiency (EQE, red) and specific detectivity (D*, green) at V_{ds} = 1 V

of MoS_2 photodetectors and make this hybrid photodetector a suitable candidate for practical applications. To evaluate long-term stability of the hybrid photodetector, we measured the photocurrent of the device over 1 month (interval of 3 days), as shown in Fig. 4e; photocurrent/dark current ratio (PDCR = I_{ph}/I_{dark}) was applied. After being exposed to air for 1 month, PDCR of the device shows no obvious degeneration; inserted images show that the current measured at day 1 and day 31 almost remains on the same level; clearly, this hybrid photodetector has good stability for long-term photodetection.

Photoresponse Mechanism

Here we investigated the mechanism on the photodetection performance enhancement of the ZnO-QDs/MoS_2 photodetector. Firstly, we checked the absorption of the hybrid structure by means of numerical simulations. Using the finite element method, we built a calculation model that consists of an air domain on top and a sapphire substrate at beneath. The top and bottom of the model were truncated by two perfectly matched layers to avoid spurious reflections. The refractive index of the sapphire substrate was set as a constant 1.75. In the beginning, we respectively put 0.8-nm-thick MoS_2 layer and 4.5-nm-thick ZnO layer on the sapphire substrate, to check the independent absorptions. The refractive index of MoS_2 monolayer was taken from reference [36], and the one for ZnO was taken from reference [37]. We then put a hybrid layer (ZnO over MoS_2) on the same sapphire substrate to examine the overall absorption. As shown in Fig. 5a, the hybrid layer presents an enhanced absorption at the wavelength region below than 400 nm compared with the bare MoS_2 monolayer, revealing a better UV absorption after the ZnO-QDs decoration. Then, we experimentally checked UV-Vis absorption spectra of MoS_2, ZnO-QDs, and ZnO-QDs/MoS_2 and the result is matched to the

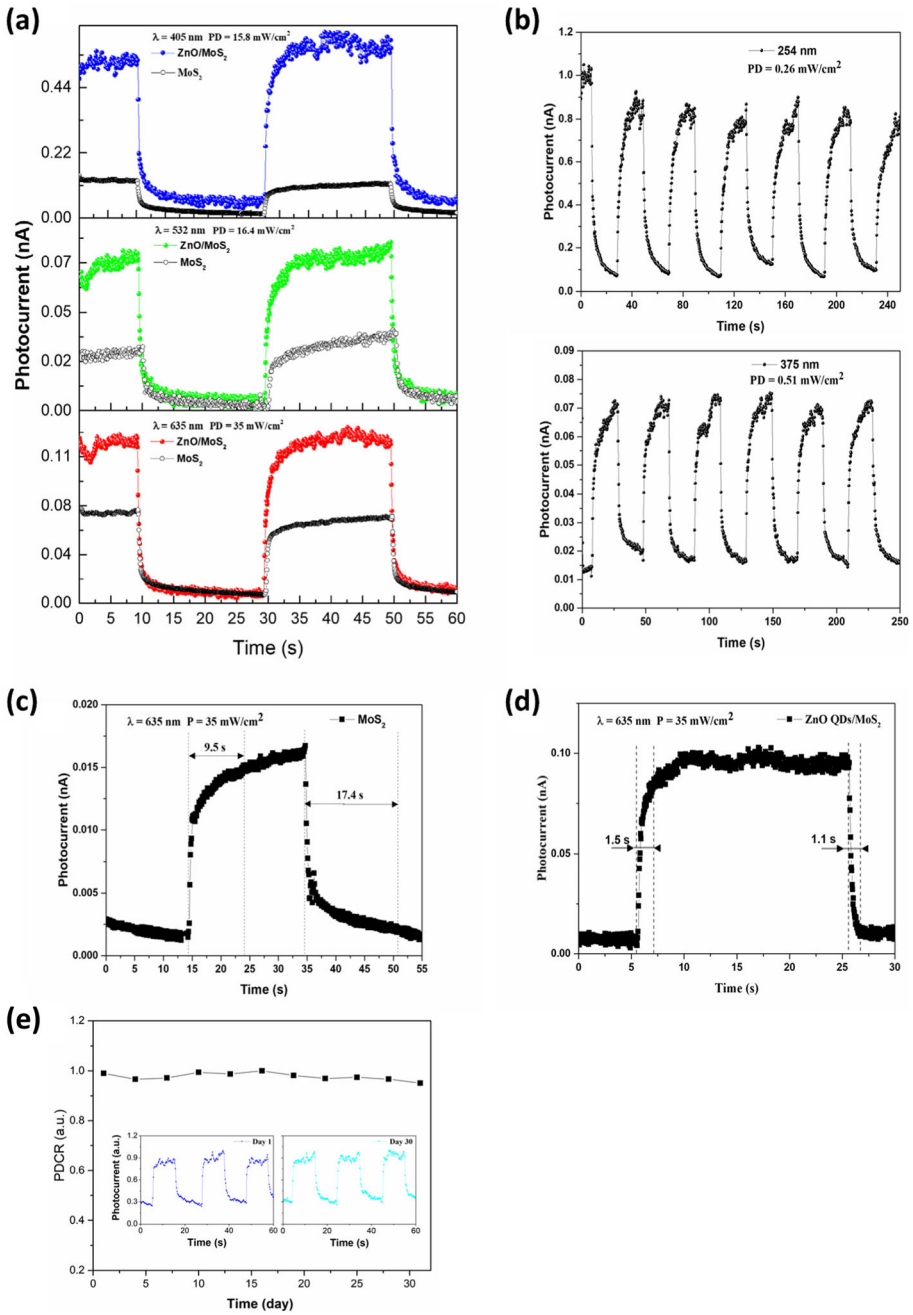

Fig. 4 **a** Photocurrent of pristine device and ZnO-QDs/MoS_2 photodetector illuminated under different PD with different wavelength at V_{ds} = 1 V. **b** Multiple cycles of photoresponse of the ZnO-QDs/MoS_2 photodetector under DUV (254 nm) and UV (375 nm) light illumination (V_{ds} = 1 V). The response time of **c** pristine device and **d** ZnO-QDs/MoS_2 photodetector illuminated under PD of 35 mW/cm^2 with wavelength of 635 nm at V_{ds} = 1 V. **e** Normalized PDCR of ZnO-QDs/MoS_2 photodetector under a 532-nm laser illumination at V_{ds} = 1 V; photocurrent measured at day 1 and day 31 was inserted for better comparison

calculated one. As shown in Fig. 5b, monolayer MoS_2 exhibits a broadband absorption range from UV to visible wavelength light and no absorption peaks are found when the wavelength increases to NIR. As for ZnO-QDs, the absorption peaks are located at UV wavelength light and there exists a larger absorption rate in comparison with MoS_2. After decoration of ZnO-QDs, we found that ZnO-QDs/MoS_2 exhibits stronger absorption ability than pristine MoS_2, indicating that the heterostructure has more intensive light-matter interaction. The corresponding Tauc plots are shown in Fig. 5c, and the band gap of MoS_2 and ZnO-QDs can be calculated

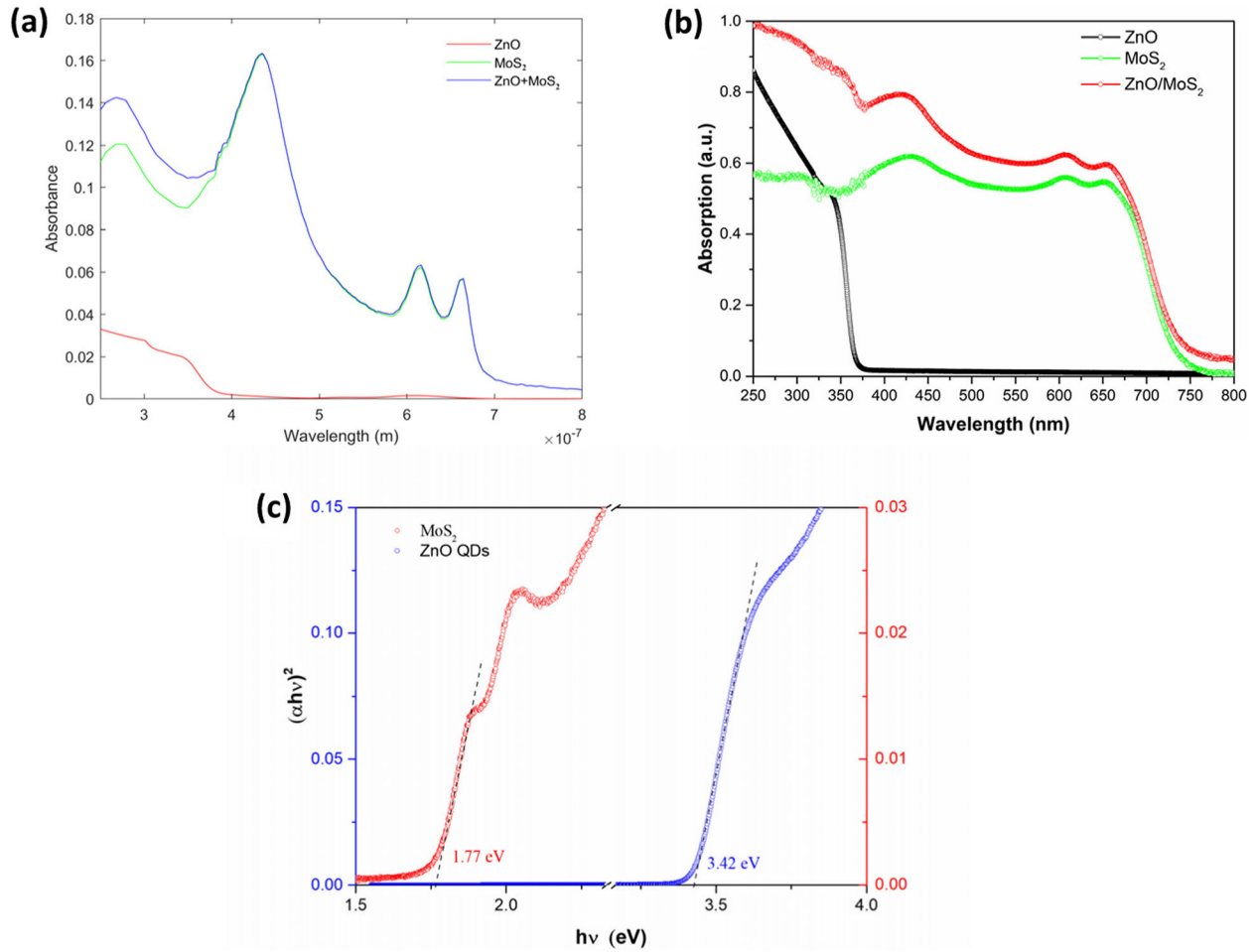

Fig. 5 **a** Calculated absorption spectra of MoS_2, ZnO-QDs, and ZnO-QDs/MoS_2. **b** UV-vis absorption spectra of MoS_2, ZnO-QDs, and ZnO-QDs/MoS_2. **c** Tauc plots of MoS_2 and ZnO-QDs

to be ~ 1.77 eV and ~ 3.42 eV, respectively, which are close to the values in the previous reports [27, 38].

Based on the previous reports, MoS_2 and ZnO-QDs are both n-type semiconductors with the work function of 4.7 eV and 5.3 eV [39, 40], respectively. Electron affinity of MoS_2 is approximately 4.3 eV [41], which is slightly larger than that of ZnO-QDs (4.2 eV) [42]. Band gap of MoS_2 and ZnO-QDs is considered to be 1.8 eV and 3.4 eV according to Tauc plot calculations. The energy band structure of MoS_2 and ZnO (before and after contact), shown in Fig. 6a and b, is constructed and used to investigate the mechanism about the photodetection performance enhancement.

MoS_2/ZnO-QDs heterojunction is formed by Van der Waals forces and the I-type band alignment at the interface can be used to explain the enhanced responsivity [42]. When these heterostructures are illuminated under UV light, both ZnO-QDs and MoS_2 strongly absorb light photon and electrons move from valence to conduction band so that the process "I" occurs. Afterwards, electrons are injected from ZnO-QDs conduction band into MoS_2 conduction band so as to form process "V" through thermal agitation, meanwhile, part of electrons in ZnO-QDs conduction band tunnel to conduction band in MoS_2, resulting in the process "III." And then, holes in ZnO-QDs valence band move to the corresponding valence band in MoS_2, as shown in the process "IV." Also, spontaneous emission can make some of the electrons in the conduction band of ZnO-QDs and move back to the valence band to emit photon that can excite electrons in the valence band of MoS_2 to the conduction band so as to form the process "II." On the other hand, similar processes happened when the hybrid devices were illuminated by visible light, except the excited electrons were from defect energy level of ZnO-QDs [43], which would lower excited energy. As a result, these excited electron-hole pairs transfer from ZnO-

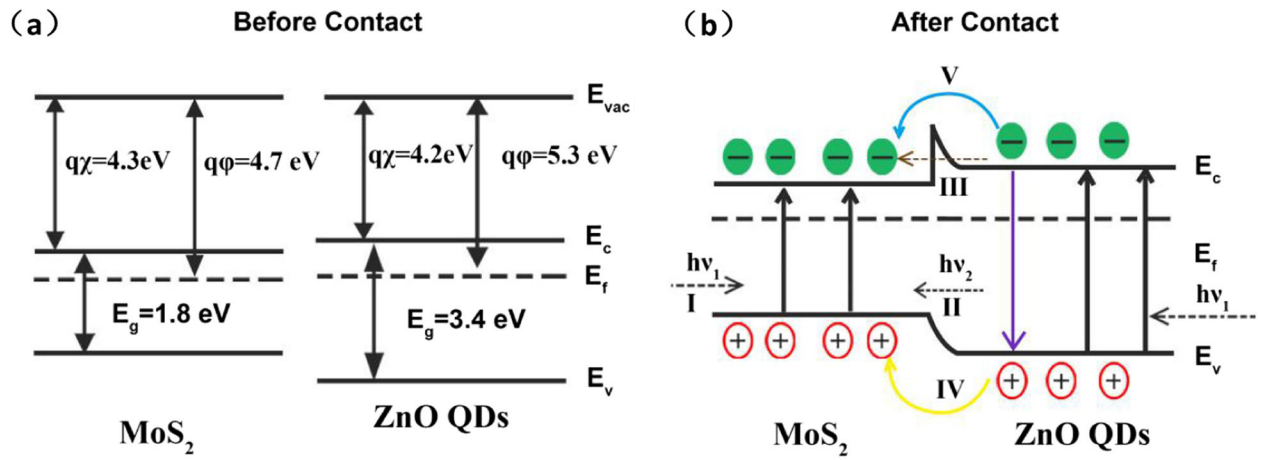

Fig. 6 **a** and **b** are band diagrams of MoS_2 and ZnO-QDs before and after contact

QDs to MoS_2 and lead to significant enhancement of photocurrent in comparison with the pristine device. In addition, large number of excited carries MoS_2 will greatly increase the recombination rate and decrease the response and decay time [42], which were observed in Fig. 4c and d.

Conclusions

In summary, we report a photodetector based on monolayer MoS_2/ZnO-QDs hybrid structure. Compared with the monolayer MoS_2, ZnO-QDs decoration leads to not only huge enhancement of photoresponse in visible spectrum but also extension to deep ultraviolet (DUV) range. Under excitation of visible light, this hybrid device exhibits faster response speed (1.5 s and 1.1 s, respectively), higher responsivity over 0.084 A/W, and larger detectivity of 1.05×10^{11} Jones. These are attributed to large number of injection of carries from ZnO-QDs to MoS_2. In addition, the hybrid device shows excellent stability under exposure to atmosphere at room temperature. Thus, our study may provide a method to improve the performance of photodetectors and expand the building blocks for high-performance optoelectronic devices.

Abbreviations

PL: Photoluminescence; AFM: Atomic force microscopy; XPS: X-ray photoelectron spectra; CVD: Chemical vapor deposition; R_λ: Responsivity; I_{ds}: Source-drain current; I_{ph}: Photocurrent; EQE: External quantum efficiency; D*: Detectivity; VB: Valence band; CB: Conduction band

Acknowledgements

We acknowledged Prof. Zheng Zhaoqiang from Guangdong Technology University who gave us many suggestions to measure the photodetector.

Authors' contributions

Yong Heng Zhou is the first author who designed the device and wrote this manuscript. Zhi Bin Zhang is the second author who fabricates and measures this device. Ping Xu and Han Zhang give some suggestions for this manuscript. Bing Wang is the corresponding author. All authors read and approved the final manuscript.

Authors' information

Yong Heng Zhou is a Graduate Student in Shenzhen University, majoring in optic-electronic devices field.
Zhi Bin Zhang is a Graduate Student in Shenzhen University, majoring in optic-electronic devices field.
Ping Xu is a Professor in Shenzhen University, majoring in optic-electronic research.
Han Zhang is a Professor in Shenzhen University, majoring in optic-electronic research.
Bing Wang is an Associate Professor in Shenzhen University, majoring in optic-electronic research such as photodetector and gas sensor.

Funding

This work was supported by the National Natural Science Foundation of China (50902097) and Guangdong Natural Science Foundation of China (2019A1515010007).

Availability of data and materials

In the manuscript, all data supporting their findings are from the fabrication experimental, characterization, and measurement. All authors wish to share their data. The data can be shared.

Competing interests

The authors declare that they have no competing interests.

Received: 20 June 2019 Accepted: 14 October 2019
Published online: 04 December 2019

References

1. Thanga Gomathi P, Sahatiya P, Badhulika S (2017) Large-area, flexible broadband photodetector based on ZnS–MoS_2 hybrid on paper substrate. Adv Funct Mater 27:1701611
2. Mu H, Wang Z, Yuan J et al (2015) Graphene-Bi_2Te_3 heterostructure as saturable absorber for short pulse generation[J]. ACS Photonics 2(7): 150608131013000
3. Jiang X, Liu S, Liang W et al (2018) Broadband nonlinear photonics in few-layer MXene $Ti_3C_2T_x$ (T = F, O, or OH)[J]. Laser Photonics Rev 12(2):1700229

4. Yao JD, Zheng ZQ, Yang GW (2019) Production of large-area 2D materials for high-performance photodetectors by pulsed-laser deposition[J]. Prog Mater Sci 100573
5. Yao J, Zheng Z, Yang G (2017) All-layered 2D optoelectronics: a high-performance UV–vis–NIR broadband SnSe photodetector with Bi2Te3 topological insulator electrodes[J]. Adv Funct Mater 27(33):1701823
6. Hu K, Chen H, Jiang M, Teng F, Zheng L, Fang X (2016) Broadband photoresponse enhancement of a high performance t -Se microtube photodetector by plasmonic metallic nanoparticles. Adv Funct Mater. 26: 6641–6648
7. Um D-S, Lee Y, Lim S, Park J, Yen W-C, Chueh Y-L, Kim H-j, Ko H (2016) InGaAs nanomembrane/Si van der Waals heterojunction photodiodes with broadband and high photoresponsivity. ACS Appl. Mater. Interfaces 8: 26105–26111
8. Sichao D, Lu W, Ali A, Zhao P, Shehzad K, Guo H, Ma L, Liu X, Pi X, Wang P, Fang H, Xu Z, Gao C, Dan Y, Tan P, Wang H, Lin C-T, Yang J, Dong S, Cheng Z, Li E, Yin W, Luo J, Yu B, Hasan T, Xu Y, Hu W, Duan X (2017) A broadband fluorographene photodetector. Adv Mater 29:1700463
9. Yao J, Zheng Z, Yang G (2018) Ultrasensitive 2D/3D heterojunction multicolor photodetectors: a synergy of laterally and vertically aligned 2D layered materials[J]. ACS Appl Mater Interfaces 10(44):38166–38172
10. Yao J, Yang G (2018) Flexible and high-performance all-2D photodetector for wearable devices[J]. Small 14(21):1704524
11. Xu H, Han X, Dai X et al (2018) High detectivity and transparent few-layer MoS2/glassy-graphene heterostructure photodetectors[J]. Adv Mater 30(13):1706561
12. Zhang X, Grajal J, Vazquez-Roy JL et al (2019) Two-dimensional MoS2-enabled flexible rectenna for Wi-Fi-band wireless energy harvesting[J]. Nature 566(7744):368
13. Zhu J, Xu H, Zou G et al (2019) MoS2–OH bilayer-mediated growth of inch-sized monolayer MoS2 on arbitrary substrates[J]. J Am Chem Soc 141(13): 5392–5401
14. Wang Y, Huang X, Wu D, Zhuo R, Wu E, Cheng J, Shi Z, Xu T, Tiana Y, Li X (2018) A room-temperature near-infrared photodetector based on a MoS_2/CdTe p–n heterojunction with a broadband response up to 1700 nm. J Mater Chem C 6:4861–4865
15. Lu L, Liang Z, Wu L et al (2017) Few-layer bismuthene: sonochemical exfoliation, nonlinear optics and applications for ultrafast photonics with enhanced stability[J]. Laser Photonics Rev 1700221:5
16. Yupeng Z, Chang-Keun L, Zhigao D, GuannanYu, Haus JW, Han Z, Paras N Prasad (2019) Photonics and optoelectronics using nano-structured hybrid perovskite media and their optical cavities, Phys. Rep 795(10):1–51
17. Huang Y, Zhan X, Xu K, Yin L, Cheng Z, Jiang C, Wang Z, He J (2016) Highly sensitive photodetectors based on hybrid 2D-0D SnS_2-copper indium sulfide quantum dots. Appl Phys Lett 108:013101
18. Lu L, Tang X, Cao R et al (2017) Broadband nonlinear optical response in few-layer antimonene and antimonene quantum dots: a promising optical Kerr media with enhanced stability[J]. Adv Opt Mater 5(17):1700301
19. Zheng Z, Yao J, Zhu L et al (2018) Tin dioxide quantum dots coupled with graphene for high-performance bulk-silicon Schottky photodetector[J]. Mater Horizons 5(4):727–737
20. Boruah BD, Misra A (2015) ZnO quantum dots and graphene based heterostructure for excellent photoelastic and highly sensitive ultraviolet photodetector. RSC Adv 5:90838–90846
21. Son DI, Yang HY, Kim TW, Park WI (2013) Photoresponse mechanisms of ultraviolet photodetectors based on colloidal ZnO quantum dot-graphene nanocomposites. Appl Phys Lett. 102:021105
22. Lin KF, Cheng HM, Hsu HC, Lin LJ, Hsieh WF (2005) Band gap variation of size-controlled ZnO quantum dots synthesized by sol–gel method. Chem Phys Lett. 409:208
23. Mahyavanshi RD, Kalita G, Ranade A, et al (2018) Photovoltaic action with broadband photoresponsivity in germanium-MoS2 ultrathin heterojunction. IEEE Transections on Electron Devices. 65(10):4434–4440
24. Zhuo R, Wang Y, Wu D, et al (2017) High-performance self-powered deep ultraviolet photodetector based on MoS2/GaN p–n heterojunction. Journal of Materials Chemistry C. 6(2):299–303
25. Wang J, Cai X, Shi R, et al (2017) Twin defect derived growth of atomically thin MoS2 dendrites. ACS Nano. 12(1):635–643
26. Lee C, Yan H, Brus LE et al (2010) Anomalous lattice vibrations of single- and few-layer MoS_2. ACS Nano 4(5):2695–2700
27. Mishra R, Yadav RS, Pandey AC et al (2010) Formation of ZnO@$Cd(OH)_2$, core-shell nanoparticles by sol–gel method: an approach to modify surface chemistry for stable and enhanced green emission. J Luminescence 130(3): 365–373
28. Zhou X, Gan L, Tian W, Zhang Q, Jin S, Li H, Bando Y, Golberg D, Zhai T (2015) Ultrathin $SnSe_2$ flakes grown by chemical vapor deposition for high-performance photodetectors. Adv Mater. 27:8035–8041
29. Hu X, Zhang X, Liang L, Bao J, Li S, Yang W, Xie Y (2014) High-performance flexible broadband photodetector based on organolead halide perovskite. Adv Funct Mater. 24(46):7373–7380
30. Zheng Z, Yao J, Xiao J, Yang G (2016) Synergistic effect of hybrid multilayer In_2Se_3 and nanodiamonds for highly sensitive photodetectors. ACS Appl. Mater. Interfaces. 8(31):20200–20211
31. Zhang W, Huang JK, Chen CH et al (2013) High-gain phototransistors based on a CVD MoS_2 monolayer. Advanced Materials 25(25):3456–3461
32. Sun M, Fang Q, Xie D et al (2018) Heterostructured graphene quantum dot/WSe2/Si photodetector with suppressed dark current and improved detectivity[J]. Nano Res. 1–11(6):3233–3243
33. Kim CO, Hwang SW, Kim S, et al (2015) High-performance graphene-quantum-dot photodetectors[J]. Sci Rep. 4:5603
34. Li X, Zhu M, Du M et al (2016) High detectivity graphene-silicon heterojunction photodetector[J]. Small 12(5):549–549
35. Qin JK, Ren DD, Shao WZ et al (2017) Photoresponse enhancement in monolayer ReS_2 phototransistor decorated with CdSe-CdS-ZnS quantum dots. ACS Appl Mater Interfaces
36. Jung G H, Yoo SJ, Park QH. Measuring the optical permittivity of two-dimensional materials without a priori knowledge of electronic transitions. Nanophotonics 8 (2018).
37. Stelling C, Singh CR, Karg M et al (2017) Plasmonic nanomeshes: their ambivalent role as transparent electrodes in organic solar cells. Sci Rep 7: 42530
38. Mak KF, Lee C, Hone J et al (2010) Atomically thin MoS_2: a new direct-gap semiconductor. Phys Rev Lett 105(13):136805
39. Yin Z, Li H, Li H et al (2012) Single-layer MoS_2 phototransistors. ACS Nano 6(1):74–80
40. Zhao S, Wang G, Liao J et al (2018) Vertically aligned MoS_2/ZnO nanowires nanostructures with highly enhanced NO_2, sensing activities. Appl Surf Sci
41. Xue F, Chen L, Chen J et al (2016) type MoS_2 and n-type ZnO diode and its performance enhancement by the piezophototronic effect. Advanced Materials 28(17):3391–3398
42. Nazir G, Khan MF, Akhtar I et al (2017) Enhanced photoresponse of ZnO quantum dot-decorated MoS_2 thin films. RSC Adv 7(27):16890–16900
43. Oba F, Togo A, Tanaka I (2008) Defect energetics in ZnO: a hybrid Hartree-Fock density functional study. Phys. Rev. B. 77(24):245202

Publisher's Note